Available online at www.sciencedirect.com
ScienceDirect
Thermochimica Acta 456 (2007) 48–55
thermochimica acta
www.elsevier.com/locate/tca

The kinetic analysis of non-isothermal nickel oxide reduction in hydrogen atmosphere using the invariant kinetic parameters method

B. Janković *, B. Adnađević, S. Mentus

Faculty of Physical Chemistry, University of Belgrade, Studentski trg 12-16, P.O. Box 137, 11001 Belgrade, Serbia and Montenegro

Received 24 October 2006; received in revised form 22 December 2006; accepted 28 January 2007
Available online 3 February 2007

Abstract

The powder sample of nickel oxide was synthesized by sol–gel procedure. The non-isothermal reduction of nickel oxide using hydrogen, was investigated by temperature-programmed reduction (TPR) at four different heating rates (2.5, 5, 10 and 20 °C min^{-1}). The kinetics parameters (E_a, ln$A$) were determined using Friedman (FR) isoconversional method and the invariant kinetic parameters method (IKP). The IKP method was applied in the conversion range of $0.20 \leq \alpha \leq 0.60$. The activation energy value obtained by the IKP method ($E_a = 96.4$ kJ mol^{-1}) is somewhat higher than the value obtained by Friedman's method ($E_a = 90.8$ kJ mol^{-1}). The values of invariant kinetic parameters were used for numerical evaluation of conversion function, $f(\alpha)$. The kinetic model of the investigated reduction process was determined, and this model corresponds to the empirical two-parameter Šesták–Berggren equation, which gives a more quantitative description. The kinetic triplet obtained for the investigated process is: $E_a = 96.4$ kJ mol^{-1}; $A = 1.04 \times 10^8$ min^{-1} and $f(\alpha) = \alpha^{0.63}(1-\alpha)^{1.39}$. In agreement with the obtained results, the mechanism of nickel oxide reduction by hydrogen was considered.

Keywords: Invariant kinetic parameters method (IKP); Nickel oxide; Reduction; Activation energy; Šesták–Berggren kinetic model

1. Introduction

Metal oxides are used as catalysts in a large variety of commercial processes for the conversion of hydrocarbons [1,2]. Selective oxidation, ammoxidation, and selective dehydrogenation probably constitute the most important catalytic applications of metal oxides [2]. In addition, due to their low cost, metal oxides are also used as supports of many other catalytic materials (metals, sulfides, carbides, nitrides, etc.) [1,2]. In most cases, pure stoichiometric oxides do not exhibit high catalytic activity [2]. For the preparation of active oxide catalysts, the partial reduction of nickel oxide under hydrogen at elevated temperatures is the effective method for this preparation [3–5]. In general terms, two different kinetic models have been proposed for the reduction of oxides: the "nucleation model" [4,6] and the "interface-controlled model" [7]. The first reported systematic measurement of bulk NiO reduction was by Benton and Emmett [8]. These authors measured water formation as an indication of the extent of reaction for a sample of NiO made by heating nickel nitrate at 400 °C. They were approached to some very important conclusions and these are: (a) reduction occurs at the interface between NiO and previously reduced Ni; (b) there is an "autocatalytic" effect; (c) there is an induction (i.e. nucleation) period that depends on the nature of the sample and temperature; and (d) added water reduces the reduction rate and increases the induction period. Koga and Harrison, reviewed general reactions between solids and hydrogen and represented the induction process as generation of nickel atoms on the outer surface of NiO grains [9]. Following nucleation, Ni clusters grow two-dimensionally across the surface until they overlap, at which point hydrogen rapidly dissociates on Ni and the interface proceeds quikly into the grain [9]. Bandrowski et al. [10] measured water produced during the reduction to generate sigmoidal conversion curves they explained with a two-step kinetic model. The first step, reaction between NiO and hydrogen atoms adsorbed on NiO, predominates in the early part of the reduction and is proportional to the square root of the hydrogen pressure. The second step is reaction at the metal–oxide interface between NiO and hydrogen atoms adsorbed on the previously reduced NiO. The above models emphasized the chemical mechanism and kinetics

* Corresponding author. Tel.: +381 11 187 133; fax: +381 11 187 133.
E-mail address: bojanjan@ffh.bg.ac.yu (B. Janković).

0040-6031/$ – see front matter © 2007 Elsevier B.V. All rights reserved.
doi:10.1016/j.tca.2007.01.033

of the reduction process, but there was a little uniformity in the physical properties of NiO grains and pellets used. Nevertheless, it was suspected that morphological factors were just as important as topological properties in the determining the course of the reduction. These factors were demonstrated by Moriyama and Yamaguchi [11], who found that reduction rate constants were inversely proportional to grain size above a diameter of about 10 μm. Such dependence is predicted by the shrinking core model [12]. Richardson et al. [13] conducted a series of experiments using isothermal H_2 consumption and magnetization measurements to determine the Ni–O bond rupture (NiO conversion) and the growth of nucleated Ni atoms, respectively. They found the growth process lagged NiO conversion by a time interval that increased with decreasing temperature, lower gas flow rates and the presence of H_2O added to the reducing gas. Rodriguez et al. [14] showed that in experiments with NiO (1 0 0) crystal and NiO powders, oxide reduction is observed at atmospheric pressures and elevated temperatures (250–350 °C), but only after an induction period. These authors showed that the presence of O vacancies lead to an increase in the adsorption energy of H_2 and substantially lowers the energy barrier associated with the cleavage of the H–H bond. Richardson et al. [15] studied the hydrogen reduction of porous bulk NiO particles with in situ hot-stage X-ray diffraction (XRD) in the temperature range 175–300 °C. The results obtained by these authors indicated that reduction in the absence of water added to the reducing gas followed several steps: (1) an induction period associated with the initial reduction of NiO and the appearance of Ni metal clusters; (2) acceleration of the reduction rate as the size of the clusters increase; and (3) a pseudo-first-order process in which NiO disappeared and Ni appeared in concert until reduction slowed at a fractional conversion of about 0.8. When 2.2×10^{-2} atm of H_2O was added to the reducing gas, induction time increased by approximately a factor of two and the reduction rate decreased, with an apparent activation energy of $126 \pm 27\,\mathrm{kJ\,mol^{-1}}$ compared to $85 \pm 6\,\mathrm{kJ\,mol^{-1}}$ without added water [15]. Utigard et al. [16] investigated the reduction kinetics of NiO granules formed by vapour deposition from a chloride solution, using thermal gravimetry. They reported that in the temperature range from 400 to 600 °C, the rate of reduction increased with increasing temperature and increasing hydrogen pressure. Microscopic analysis showed that in this temperature range the reaction followed the shrinking core model [16]. The same authors found that the activation energy for reduction process have a value of $90\,\mathrm{kJ\,mol^{-1}}$, in the above temperature range. Based on the facts given above, in this paper, the kinetics and mechanism of powder nickel oxide reduction, which was obtained by gel-combustion procedure with hydrogen at the atmospheric pressure was investigated by temperature-programmed reduction (TPR).

2. Experimental procedure

2.1. Materials and methods

The NiO samples were obtained by gel-combustion method described elsewhere [17]. A green-colored transparent gel was obtained by drying an aqueous solution of nickel nitrate hexahydrate (Fluka, 99.5%) and citric acid (Fluka, 99.5%), dissolved in a mole ratio of 1.8:1. This gel further underwent a self-ignition by heating in air up to 300 °C, and by an additional heating up to 500 °C which produce a very fine nickel oxide powders.

2.2. Thermogravimetric measurements

The experiments were carried out in a TA SDT 2960 device, capable of simultaneous TGA-DTA analysis in the temperature range from 25 to 1500 °C. The nickel oxide samples were reduced directly within the thermobalance, in korund pans, under (99.9995 vol.%) hydrogen flowing at a rate of $100\,\mathrm{mL\,min^{-1}}$, and using various heating rates: 2.5, 5, 10 and $20\,^{\circ}\mathrm{C\,min^{-1}}$, in the temperature range from an ambient one up to 500 °C. The sample mass used for thermogravimetric investigations was about 25 ± 0.5 mg.

3. Kinetic analysis

Experimental data for the kinetic analysis of heterogeneous solid–gas reactions can be obtained under different conditions. We here analyse the data obtained under non-isothermal conditions, with a linear regime of temperature increase in time ($\beta = \mathrm{d}T/\mathrm{d}t = const.$, where β is the heating rate, T is the temperature, and t is the time). Under such conditions, for a heterogeneous solid–gas reaction, occurring in a single step, the reaction rate is expressed by the well-known general equation [18]:

$$\frac{\mathrm{d}\alpha}{\mathrm{d}t} \equiv \beta\frac{\mathrm{d}\alpha}{\mathrm{d}t} = Af(\alpha)\exp\left(-\frac{E_a}{RT}\right) \quad (1)$$

where α is the degree of conversion, A is the pre-exponential factor, E_a is the activation energy, $f(\alpha)$ is the differential conversion function and R is the gas constant. The use of Eq. (1) supposes that a kinetic triplet (E_a, A, $f(\alpha)$) describes the time evolution of a physical or chemical change.

3.1. The methods used to evaluate the kinetic parameters

3.1.1. Friedman method [19] (FR method)

The differential isoconversional method suggested by Friedman [19] is based on the general form of rate equation, written in its logarithmic form:

$$\ln\frac{\mathrm{d}\alpha}{\mathrm{d}t} \equiv \ln\,\beta\frac{\mathrm{d}\alpha}{\mathrm{d}T} = \ln\,Af(\alpha) = \frac{E_a}{RT} \quad (2)$$

For $\alpha = const.$, the plot of $\ln(\mathrm{d}\alpha/\mathrm{d}t)$ versus $1/T$, obtained from thermograms recorded at several heating rates, should be a straight line whose slope allows an evaluation of the activation energy.

3.1.2. The invariant kinetic parameters method [20,21] (IKP method)

The IKP method is based on the observation [22,23] that the same experimental curve $\alpha = \alpha(T)$ can be described rela-

Table 1
Expressions for $f(\alpha)$ and $g(\alpha)$ functions for some of the common mechanisms operating in the solid state reactions

No.	Symbol	Reaction model	$f(\alpha)$	$g(\alpha)$
1	P1	Power law	$4\alpha^{3/4}$	$\alpha^{1/4}$
2	P2	Power law	$3\alpha^{2/3}$	$\alpha^{1/3}$
3	P3	Power law	$2\alpha^{1/2}$	$\alpha^{1/2}$
4	P4	Power law	$2/3\alpha^{-1/2}$	$\alpha^{3/2}$
5	R1	Zero-order (Polany–Winger equation)	1	α
6	R2	Phase-boundary controlled reaction (contracting area, i.e. bidimensional shape)	$2(1-\alpha)^{1/2}$	$[1-(1-\alpha)^{1/2}]$
7	R3	Phase-boundary controlled reaction (contracting volume, i.e. tridimensional shape)	$3(1-\alpha)^{2/3}$	$[1-(1-\alpha)^{1/3}]$
8	F1	First-order (Mampel)	$(1-\alpha)$	$-\ln(1-\alpha)$
9	F3/2	Three-halves order	$(1-\alpha)^{3/2}$	$2[(1-\alpha)^{-1/2}-1]$
10	F2	Second-order	$(1-\alpha)^2$	$(1-\alpha)^{-1}-1$
11	F3	Third-order	$(1-\alpha)^3$	$(1/2)[(1-\alpha)^{-2}-1]$
12	A1/2	Avrami–Erofe'ev ($r=0.5$)	$(1/2)(1-\alpha)[-\ln(1-\alpha)]^{-1}$	$[-\ln(1-\alpha)]^2$
13	A3/2	Avrami–Erofe'ev ($r=1.5$)	$(3/2)(1-\alpha)[-\ln(1-\alpha)]^{1/3}$	$[-\ln(1-\alpha)]^{2/3}$
14	A2	Avrami–Erofe'ev ($r=2$)	$2(1-\alpha)[-\ln(1-\alpha)]^{1/2}$	$[-\ln(1-\alpha)]^{1/2}$
15	A3	Avrami–Erofe'ev ($r=3$)	$3(1-\alpha)[-\ln(1-\alpha)]^{2/3}$	$[-\ln(1-\alpha)]^{1/3}$
16	A4	Avrami–Erofe'ev ($r=4$)	$4(1-\alpha)[-\ln(1-\alpha)]^{3/4}$	$[-\ln(1-\alpha)]^{1/4}$
17	D1	One-dimensional diffusion	$1/2\alpha$	α^2
18	D2	Two-dimensional diffusion (bidimensional particle shape) Valensi equation	$1/[-\ln(1-\alpha)]$	$(1-\alpha)\ln(1-\alpha)+\alpha$
19	D3	Three-dimensional diffusion (tridimensional particle shape) Jander equation	$3(1-\alpha)^{1/3}/2[(1-\alpha)^{-1/3}-1]$	$[1-(1-\alpha)^{1/3}]^2$
20	D4	Three-dimensional diffusion (tridimensional particle shape) Ginstling–Brounshtein	$3/2[(1-\alpha)^{-1/3}-1]$	$(1-2\alpha/3)-(1-\alpha)^{2/3}$

tively correct by several functions of conversion and, for a single $\alpha=\alpha(T)$ curve, the values of the activation parameters, obtained for various analytical forms of $g(\alpha)$, are correlated through an apparent compensation effect.

$$\ln A = \alpha^* + \beta^* E_a \tag{3}$$

where α^* and β^* are constants (the compensation effect parameters).

In order to apply this method for a given heterogeneous reaction, $\alpha=\alpha(T)$ curves for several heating rates (β_v, $v=1, 2, 3, \ldots$) should be recorded. A set of conversion functions, g_j, $j=1,2,3, \ldots$, is also considered. The differential and integral functions of conversion used in this work are listed in Table 1.

For each heating rate β_v, using an integral or differential method, the pairs (A_{vj}, $E_{a,vj}$), characteristic for each conversion function, are determined. In this work, the Coats and Redfern [24] method was used to integrate Eq. (1). It leads to the following relation:

$$\ln\left[\frac{g_j(\alpha_{vi})}{T_{vi}^2}\right] = \ln\left(\frac{A_{vj}\,R}{\beta_v E_{a,vj}}\right) = \frac{E_{a,vj}}{RT_{vi}} \quad \text{with}$$

$$g_j(\alpha) = \int_0^{\alpha} \frac{d\alpha}{f_j(\alpha)} \tag{4}$$

where i is data point, j is the numbers of the conversion function listed in Table 1.

A plot $\ln[g_j(\alpha_{vi})/T_{vi}^2]$ versus $(1/T_{vi})$ for a given analytical form of g(α) should be a straight line whose slope and intercept allows the evaluation of activation energy and pre-exponential factor, respectively. Twenty activation energies ($E_{a,vj}$) and pre-exponential factors (A_{vj}) are calculated using the Coats and Redfern [24] method.

Using the relation of the apparent compensation effect, the compensation parameters (α_v^*, β_v^*) are determined for each heating rate. The straight lines $\ln A_v$ versus $E_{a,v}$ for several heating rates should intersect themselves in a point which corresponds to the true values of A and E_a. These were called by Lesnikovich and Levchik [20,21], the invariant activation parameters (A_{inv}, $E_{a,inv}$). Certain variations of the experimental conditions actually determine a region of intersection in the ln$A$, E_a space. For this reason, the evaluation of the invariant activation parameters is performed using the relation:

$$\ln A_{inv} = \alpha_v^* + \beta_v^* E_{a,inv} \tag{5}$$

which leads to the *super correlation* relation:

$$\alpha_v^* = \ln A_{in} - \beta_v^* E_{a,inv} \tag{6}$$

Thus, a plot α_v^* versus β_v^* is actually a straight line whose parameters allow evaluation of the invariant activation parameters.

The IKP method can be only used if E_a is independent of α [25]. On the other hand, the IKP method can be used for numerical evaluation of $f(\alpha)$, by introducing in Eq. (1) the value of the invariant kinetic parameters. Consequently, the values of $f(\alpha)$ determined by IKP method are proportional to the real $f(\alpha)$ values. In order to discriminate the kinetic model, the dependence of $f(\alpha)$ versus α obtained by IKP method and the dependence $f(\alpha)$ versus α from theoretical kinetics models can be compared. From these dependences, conclusion about the mechanism of the process can be brought, and exact expression for $f(\alpha)$ can be evaluated.

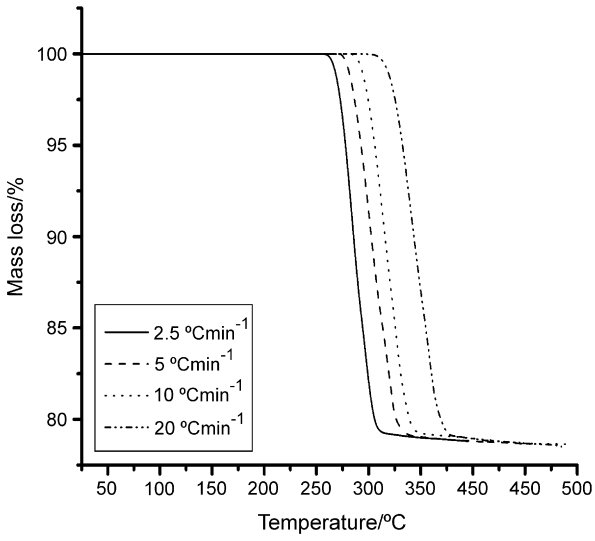

Fig. 1. TG curves for nickel oxide reduction process in hydrogen atmosphere at different heating rates.

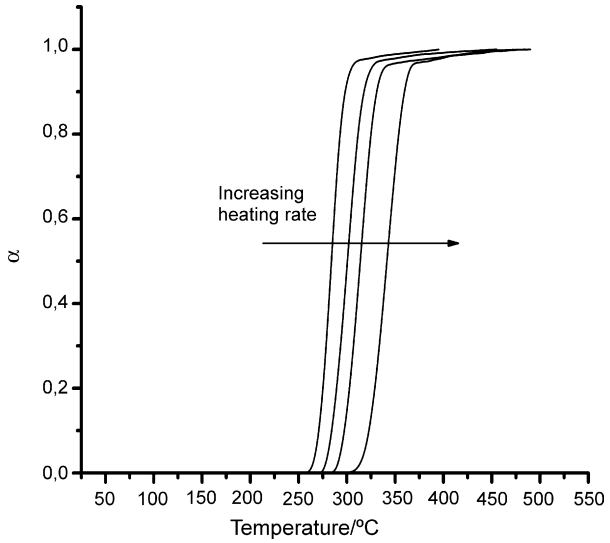

Fig. 2. The degree of conversion (α) as a function of temperature (T) for the reduction of nickel oxide under linearly rising temperature, in hydrogen atmosphere, at the following heating rates: 2.5, 5, 10 and 20 °C min^{-1} (from left to right).

4. Results and discussion

The thermogravimetric (TG) curves of the reduction process of NiO by hydrogen obtained at different heating rates (2.5, 5, 10 and 20 °C min^{-1}) are shown in Fig. 1.

The total mass-change of NiO samples at all considered heating rates is about 21.4%. The degree of conversion (α), was calculated from the TGA data, thus:

$$\alpha = \frac{m_0 - m_t}{m_0 - m_f} \tag{7}$$

where m_t represents the mass of the sample at arbitrary time t (or temperature T), whereas m_0 and m_f is the mass of the sample at the beginning and at the end of the process, respectively.

The α–T curves at different heating rates for reduction of nickel oxide in hydrogen atmosphere are shown in Fig. 2.

Table 2 shows the influence of heating rate on the characteristic temperatures of reduction process (initial temperature (T_i), inflection temperature (T_p), final temperature (T_f) and temperature differences ($\Delta T = T_f - T_i$)) (Fig. 1).

The increasing of heating rate leads to the increasing of T_i, T_p, T_f and ΔT values. Dependence of dα/dt versus T at different heating rates of the considered system is shown in Fig. 3.

With increasing of heating rate (β), the rate of reduction process of nickel oxide by hydrogen increased.

Table 2
The influence of heating rate on the characteristic temperatures of the reduction process of nickel oxide using hydrogen

β/°C min^{-1}	T_i/°C	T_p/°C	T_f/°C	ΔT/°C
2.5	260	285	395	135
5	275	300	455	180
10	285	315	465	180
20	300	340	485	185

The values of activation energies (E_a) of the investigated reduction process, at different constant values of α, which were determined by Friedman (FR) method are shown in Fig. 4.

Within the limits of the experimental errors in determination of E_a by Friedman's method, the activation energy of the reduction process of NiO in the range of $0.20 \leq \alpha \leq 0.60$ is the constant value, which is independent on α values ($E_a = 90.8$ kJ mol^{-1}). In other words, the calculated values of errors in determination of E_a vary in the range from 5.8% (±5.3 kJ mol^{-1}) to 6.0% (±5.5 kJ mol^{-1}) (Fig. 4) in considered range of α, until for $\alpha \leq 0.20$ and $\alpha \geq 0.60$, the calculated errors in E_a determination are extensively higher (Fig. 4). These results enable us to conclude that the values of E_a for $0.20 \leq \alpha \leq 0.60$ were constant and independent on α values. For $\alpha \geq 0.60$, the values of E_a increased with increasing of α values.

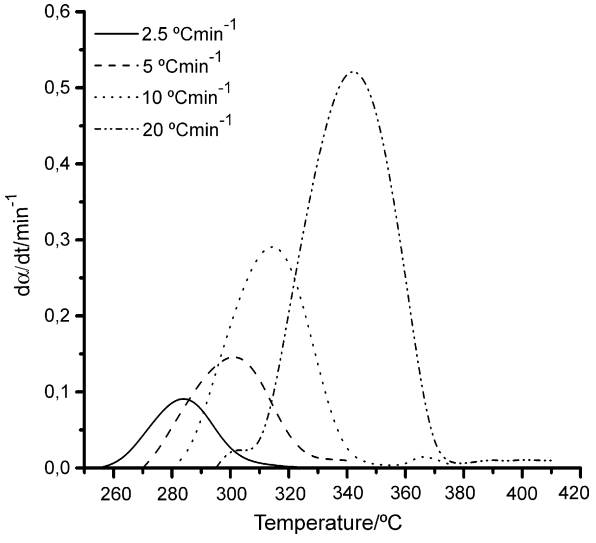

Fig. 3. Experimental (lines) reaction rates curves (dα/dt vs. T) for the reduction of nickel oxide by hydrogen at different heating rates.

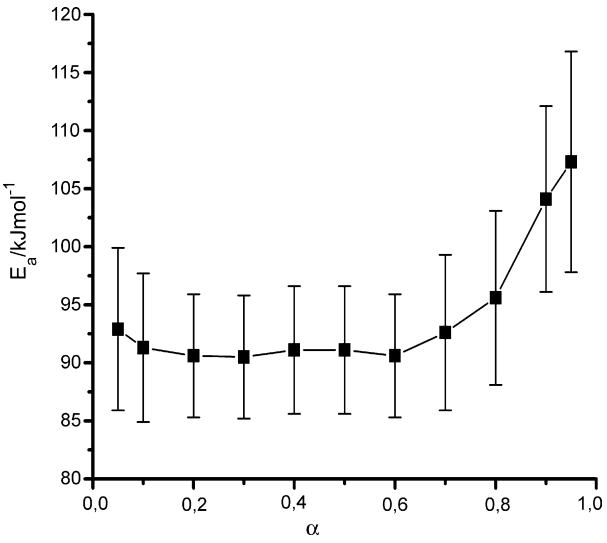

Fig. 4. Dependence of the activation energy (E_a) on the degree of conversion (α) determined using the Friedman's method for the reduction of nickel oxide by hydrogen.

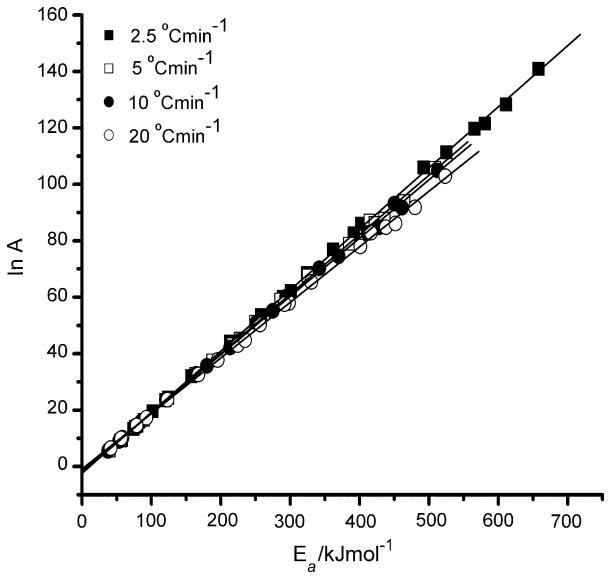

Fig. 5. Compensation effect observed between apparent activation energy and pre-exponential factor for the reduction of nickel oxide by hydrogen at different heating rates.

The obtained average value of the apparent activation energy using Friedman's method is in good agreement with values of E_a, which were determined in papers of Richardson et al. [15] (for porous powder in loosely packed samples) and Nakajima et al. [26] (for thin slab samples), respectively. From the existing of "plateau" in Fig. 4, in wide range of α values, the proof of existing of single-step reaction is evident.

The increase of E_a with increasing of α for $\alpha \geq 0.60$ (Fig. 4) designated on the existence of parallel independent reaction [27], which possessed the higher value of activation energy and whose part in the overall process in this range of α increasing.

In order to apply the IKP method, the conversion range in which the value of E_a is practically constant has to be determined and that has been done through the above methods. For determining the compensation effect parameters (α^*, β^*) Coats–Redfern method has been applied in the range of conversion where E_a is independent of the degree of conversion. The values of kinetics parameters ($\ln A$, E_a) obtained by means of Coats and Redfern method for the reduction of nickel oxide by hydrogen at different heating rates (2.5, 5, 10 and 20 °C min^{-1}) are listed in Table 3.

Calculated values of activation energies, E_a (see Table 3) are not in agreement with the values calculated by Friedman isoconversional method, what means that not one of the tested kinetic models does not correspond to the real kinetic model of reduction of nickel oxide by hydrogen. The apparent compensation effect is observed for each heating rate for the process under investigation and presented in Fig. 5.

A compensation effect of this kind is classified as a false or superficial compensation effect [28] resulting from parameter distortion by an inappropriate kinetic model function [29]. The values of α^* and β^* were calculated from the intercepts and the slopes of the straight lines obtained in the Fig. 5. The values of the apparent compensation effect (α^*, β^*) obtained at different heating rates (β) are presented in Table 4.

A linear regression from the straight-line plot of $\alpha_v^* = \ln A_{inv} - \beta_v^* E_{a,inv}$ allows computation of the invariant activation parameters (invariant pre-exponential factor A_{inv} and invariant activation energy E_{inv}). As α_v^* and β_v^* and are correlated by supercorrelation relation, one obtains: $A_{inv} = 1.04 \times 10^8$ min^{-1} and $E_{a,inv} = 96.4$ kJ mol^{-1}.

The obtained value of pre-exponential factor and corresponding temperature range of reduction process were considerable different from the values of pre-exponential factor (A) and reduction temperature ranges obtained by Richardson et al. [15] and Nakajima et al. [26]. These facts designated on the different kinetical model for reduction process of our investigated NiO samples in relation to the NiO samples, which were used in reduction experiments by the above-cited investigators.

The IKP method gives an exact value of activation energy of the investigated process, but although not one of the considered kinetic models (Table 1) does not completely kinetically described the experimental data. The values of the invariant activation parameters were used further for the numerical evaluation of $f(\alpha)$ function.

Fig. 6 shows the curves $f(\alpha)$ versus α obtained from Eq. (1) at different heating rates, with the experimental values of $\beta(d\alpha/dT)$ and the values of the invariant activation parameters.

As shown in this figure, for all observed heating rates the curves $f(\alpha)$ versus α exhibits the same shape which designates to the same reaction mechanism and shows the dependences from the heating rate (β).

It is clear from Fig. 6 that the curve of $f(\alpha)$ versus α exhibits a maximum, suggesting that the reduction of NiO by hydrogen occurs through the reaction mechanism which is similar to the mechanism represented by the Avrami–Erofe'ev equations (with $r > 1$). An inspection of the conversion functions included in Table 1 clearly confirms that only in these cases do the curves of $f(\alpha)$ against α have a maximum at $f'(\alpha_m) = 0$. The values reported for the degree of conversion at the maximum reaction rate change from $\alpha_m = 0.393$ for $r = 2$ to $\alpha_m = 0.527$ for $r = 4$ [30]. However,

Table 3
Apparent kinetic parameters for the reduction of nickel oxide in hydrogen atmosphere obtained for each kinetic function vs. the heating rates

Model[a]	$\beta = 2.5\,^{\circ}C\,min^{-1}$			$\beta = 5\,^{\circ}C\,min^{-1}$			$\beta = 10^{\circ}\,C\,min^{-1}$			$\beta = 20\,^{\circ}C\,min^{-1}$		
	$\ln A_v$	$E_{a,v}$ (kJ mol^{-1})	R	$\ln A_v$	$E_{a,v}$ (kJ mol^{-1})	R	$\ln A_v$	$E_{a,v}$ (kJ mol^{-1})	R	$\ln A_v$	$E_{a,v}$ (kJ mol^{-1})	R
1	9.38	57.6	0.9942	5.55	39.8	0.9905	5.51	37.7	0.9892	6.56	41.3	0.9921
2	14.43	79.8	0.9946	9.26	56.2	0.9915	9.03	53.5	0.9905	10.19	58.3	0.9930
3	24.40	124.4	0.9950	16.51	89.1	0.9924	15.86	85.1	0.9916	17.25	92.7	0.9938
4	82.54	391.6	0.9955	58.31	286.4	0.9934	55.17	274.9	0.9927	57.96	298.4	0.9946
5	53.63	258.0	0.9954	37.57	187.8	0.9932	35.68	180.0	0.9925	37.77	195.5	0.9944
6	60.05	289.7	0.9973	43.32	217.0	0.9964	42.17	213.5	0.9963	43.05	224.5	0.9970
7	62.17	301.0	0.9978	45.23	227.6	0.9973	44.38	225.7	0.9973	44.77	234.9	0.9976
8	68.51	324.4	0.9986	51.19	249.7	0.9985	51.02	251.6	0.9987	50.33	256.6	0.9987
9	76.93	362.0	0.9995	59.11	286.0	0.9996	60.16	294.4	0.9998	57.56	291.9	0.9996
10	85.99	402.6	0.9999	67.76	325.6	0.9999	70.26	342.0	0.9999	65.41	330.4	0.9999
11	105.96	492.3	0.9998	87.15	414.9	0.9991	93.14	450.1	0.9986	82.89	416.4	0.9995
12	140.88	658.0	0.9987	105.86	508.9	0.9986	104.88	512.9	0.9987	102.88	523.4	0.9987
13	44.23	213.3	0.9986	32.79	163.4	0.9985	32.90	164.6	0.9986	32.65	167.8	0.9986
14	31.96	157.6	0.9986	23.47	120.1	0.9984	23.72	120.9	0.9985	23.68	123.2	0.9985
15	19.56	101.9	0.9985	14.02	76.8	0.9983	14.39	77.3	0.9984	14.58	78.7	0.9984
16	13.30	74.2	0.9984	9.21	55.3	0.9981	9.65	55.6	0.9983	9.95	56.5	0.9982
17	111.33	525.2	0.9955	78.92	385.0	0.9935	74.54	369.8	0.9929	78.02	401.2	0.9947
18	119.66	565.7	0.9968	86.26	421.9	0.9956	82.73	411.6	0.9953	84.81	437.9	0.9963
19	128.27	611.2	0.9979	94.03	464.6	0.9974	91.71	461.1	0.9974	91.84	479.9	0.9977
20	121.51	580.8	0.9972	87.83	436.1	0.9963	84.70	427.9	0.9961	86.14	451.8	0.9969

[a] Enumeration of the models is given in Table 1.

the values of $f(\alpha)$ determined for the reduction of nickel oxide by hydrogen from the IKP method and shown in Fig. 6 could not be fitted exactly by any of the ideal Avrami–Erofe'ev kinetic laws included in Table 1. This behaviour can be understood if we take into account that these kinetic equations have been derived by assuming "ideal" models conditions (homogeneous particle size, shape, etc.), which are not always satisfied by real samples.

In some cases, it is convenient to use more flexible empirical kinetic model functions, $f(\alpha)$, for the description of the crystallization processes. The advantage of such an approach is that it is possible to describe experimental thermogravimetric data even in the case when some of the basic assumptions for the validity of the Avrami–Erofe'ev model are no longer held. These models can also be understood in terms of the accommodation function introduced by Šesták [31], expressing a deviation from the ideal case due to a more complex process. In this respect, it is very convenient to use the Šesták–Berggren (SB) function [32]:

$$f(\alpha) = \alpha^m(1-\alpha)^n \tag{8}$$

and this is the most popular form of $f(\alpha)$ for examination of auto-catalyzed chemical reactions. This flexible two-parameter (m, n) SB function, in fact, also includes the Avrami–Erofe'ev kinetic model. It can be shown [33] that there are combinations of parameters m and n corresponding to a given value of kinetic exponent for the Avrami–Erofe'ev model (for $r \geq 1$). Therefore, the SB kinetic model can be used for a quantitative description of more complex crystallization processes involving partially overlapping nucleation and growth phases. The kinetic parameters, m and n in Eq. (8), are characteristic of a particular crystallization process although it is rather problematic to find their real physical meaning. It was shown [34], however, that physically meaningful values of the parameter m (in Eq. (8)) should be confined in the range of $0 < m < 1$. From the complex dependence E_a on α, which is indication of the complex mechanism of nickel

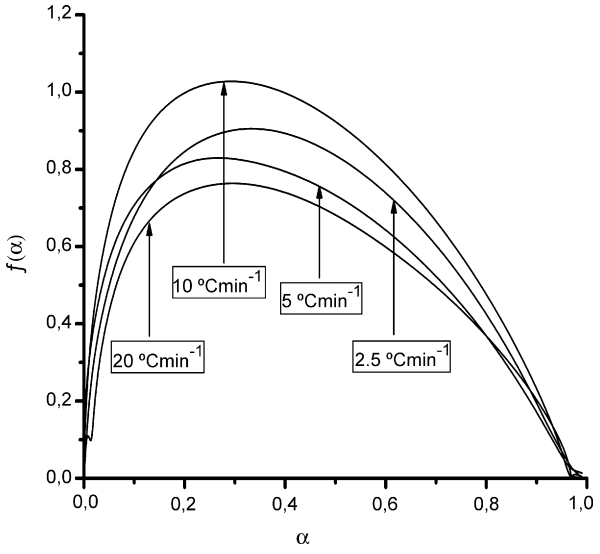

Fig. 6. Dependence of $f(\alpha)$ vs. α for the reduction of nickel oxide by hydrogen, established using invariant activation parameters at four different heating rates ($\beta = 2.5$, 5, 10 and 20 °C min^{-1}).

Table 4
Values of compensation effect parameters at four different heating rates for the reduction of nickel oxide in hydrogen atmosphere

β/°C min^{-1}	α_v^* (min^{-1})	β_v^* (mol kJ^{-1})	R
2.5	−2.4140	0.2165	0.9998
5	−1.8628	0.2109	0.9996
10	−1.4555	0.2065	0.9996
20	−0.5092	0.1968	0.9996

Table 5
The parameters of the conversion function $f(\alpha) = \alpha^m(1-\alpha)^n$ (Eq. (8)) as well as the ln$A$ value resulting from Eq. (10), for the reduction of nickel oxide samples in hydrogen atmosphere at four different heating rates

β/°C min^{-1}	m	n	α_{max}	ln$A$, A/min^{-1} [a]
2.5	0.77	1.48	0.34	19.72
5	0.46	1.22	0.27	19.10
10	0.60	1.49	0.29	19.74
20	0.69	1.39	0.33	19.44
Average	0.63	1.39	0.31	19.50

[a] Activation energy (by IKP method): 96.4 kJ mol^{-1}.

oxide reduction, the kinetic model of investigated process was determined by applying the Málek's procedure.

The kinetic exponents m, n and α_{max} satisfy the following relationship [35,36]:

$$s = \frac{m}{n} = \frac{\alpha_{max}}{1-\alpha_{max}} \quad (9)$$

where α_{max} is the value of α corresponding to the maximum of $f(\alpha)$.

Once the value of s (ratio m/n) is known, the values of the kinetic exponents m and n can be obtained using the following relation, which results from Eqs. (1) and (8):

$$\ln\left(\frac{d\alpha}{dt}\exp\left(\frac{E_a}{RT}\right)\right) = \ln A + n \ln[\alpha^s(1-\alpha)]. \quad (10)$$

The parameters of the straight lines $\ln(d\alpha/dt \cdot \exp(E_a/RT))$ versus $\ln[\alpha^s(1-\alpha)]$ are ln$A$ and n. Table 5 lists the values of kinetic exponents m and n, the values of α_{max} as well as the values of ln$A$ (with their average values) obtained by the procedure described above, for the reduction of nickel oxide in hydrogen atmosphere at different heating rates.

The values of kinetic exponents of SB model (m and n) as well as the values of α_{max} depend on the heating rates, while the values of ln$A$ do not show the significant variation with heating rates (Table 5). The values of α_{max} correspond of the maximums in Fig. 6 for SB model with kinetic exponents are given in Table 5. The obtained values of A (calculated from Table 5) at different heating rates, are in good agreement by order of magnitude with the value of A obtained using IKP method ($\times 10^8$).

On the other hand, the relationship between the values of m, n and Avrami–Erofe'ev parameter r may be obtained by equating α's from the two equations at the peak of the reaction curve where $d(d\alpha/dt)/dt = 0$ [37]. This results in the relationship:

$$r = \frac{1}{[1 + \ln(n) - \ln(n+m)]}. \quad (11)$$

The values of parameter r calculated from Eq. (11) for the investigated reduction process of NiO by hydrogen at 2.5, 5, 10 and 20 °C min^{-1} (with SB kinetics exponents from Table 5) are: 1.72, 1.47, 1.51 and 1.67, respectively.

Based on the results showed above, it was decided that indeed $f(\alpha) = \alpha^{0.63}(1-\alpha)^{1.39}$ is the best conversion function because according to Šesták et al. [38], in case of a system that contains metallic particles the reduction processes take place mainly along the border between the oxide and metallic particles.

Bearing in mind previously exhibited kinetical models and mechanisms for NiO reduction process using hydrogen (Section 1), it can be concluded with high reliability, that the reduction process occurs at the interface between NiO and previously reduced Ni without any well-ordered intermediate phase. The constant value of E_a is a consequence of constant activation energy for crystal growing of Ni crystallites, which were induced in nucleation stage of the process whose duration period depends on the heating rate of the system. The increasing of reduction rate without changing of E_a value, which is interrelationship with existing of "autocatalytic effect", i.e. it is a consequence of being proportionality between the reduction rate and area size of boundary phase of interaction. The decreasing of reduction rate and increasing of E_a values was probably caused by mutually overlapping of Ni growing crystals which lead to the decreasing of area size of boundary phase and the rate of process. The obtained values of Šesták–Berggren parameters (m, n) shows, that the increasing value of the kinetic parameter m indicates a more important role of the crystallized phase on the overall kinetics. On the other hand, the higher value of the kinetic parameter n ($n > 1$) shows the increasing complexity of the investigated reduction process. Accordingly, the proposed kinetical model for the NiO reduction process (SB model) is more complex than simple shrinking core model proposed by the authors in [12] and [16].

5. Conclusions

The kinetic process for the temperature-programmed reduction (TPR) of nickel oxide, obtained by sol–gel procedure using hydrogen has been studied. The Friedman's isoconversional method is used to yield dependency of the activation energy of reduction process on the degree of conversion. The use of the IKP method for the range where E_a is independent of α, led to the invariant activation parameters, which were used for the numerical evaluation of the conversion function ($f(\alpha)$). The activation energy (E_a) value obtained by the IKP method displays a good agreement with the value of E_a obtained by Friedman's method. It is established that the reduction of NiO using hydrogen is a multi-step mechanism and can be described by the Šesták–Berggren (SB) model.

For the temperature-programmed reduction of nickel oxide in hydrogen atmosphere, the following kinetic triplet was obtained: $E_a = 96.4$ kJ mol^{-1}, $A = 1.04 \times 10^8$ min^{-1} and $f(\alpha) = \alpha^{0.63}(1-\alpha)^{1.39}$.

Acknowledgements

The investigation was partially supported by the Ministry of Science and Environmental Protection of Serbia, under the following Projects 142025 and 142047 (S. Mentus).

References

[1] J.M. Thomas, W.J. Thomas, Principles and Practice of Heterogeneous Catalysis, New York, VCH, 1997.

[2] H.H. Kung, Transition Metal Oxides: Surface Chemistry and Catalysis, Elsevier, New York, 1989.
[3] B. Delmon, in: G. Ertl, H. Knözinger, J. Weitkamp (Eds.), Handbook of Heterogeneous Catalysis, Wiley-VCH, New York, 1997, p. 264.
[4] R.P. Furstenau, G. McDougall, M.A. Langell, Surf. Sci. 150 (1985) 55.
[5] B. Lescop, J.-Ph. Jay, G. Fanjoux, Surf. Sci. 548 (2004) 83.
[6] M.A. Langell, Surf. Sci. 164 (1985) 543.
[7] B. Delmon, Introduction á la cinétique hétérogéne, Technip, Paris, 1969 (Chapter 11).
[8] A.F. Benton, P.H. Emmett, J. Am. Chem. Soc. 46 (1924) 2728.
[9] Y. Koga, L.G. Harrison, in: C.H. Bamford, C.F.H. Tipper, R.G. Compton (Eds.), Comprehensive Chemical Kinetics, vol. 21, Elsevier, Amsterdam, 1984, p. 120.
[10] J. Bandrowski, C.R. Bickling, K.H. Yang, O.A. Hougen, Chem. Eng. Sci. 17 (1962) 379.
[11] J. Moriyama, A. Yamaguchi, Nippon Kinzoku Gakkaishi 28 (1964) 831.
[12] S. Yagi, D. Kunii, Proceedings of the 5th International Symposium on Combustion, Reinhold, New York, 1955, p. 231.
[13] J.T. Richardson, M. Lei, B. Turk, K. Forster, M.V. Twigg, Appl. Catal. A 110 (1994) 217.
[14] J.A. Rodriguez, J.C. Hanson, A.I. Frenkel, J.Y. Kim, M. Pérez, J. Am. Chem. Soc. 124 (2002) 346.
[15] J.T. Richardson, R. Scates, M.V. Twigg, Appl. Catal. A 246 (2003) 137.
[16] T.A. Utigard, M. Wu, G. Plascencia, T. Marin, Chem. Eng. Sci. 60 (2005) 2061.
[17] S. Mentus, D. Majstorović, B. Tomić, R. Dimitrijević, Mater. Sci. Forum 494 (2005) 345.
[18] See for example: F. Paulik, Special trends in thermal analysis, Chichester: Wiley, 1995 (Chapter 10).
[19] H.L. Friedman, J. Polym. Sci. C 6 (1964) 183.
[20] A.I. Lesnikovich, S.V. Levchik, J. Therm. Anal. 27 (1983) 83.
[21] A.I. Lesnikovich, S.V. Levchik, J. Therm. Anal. 30 (1985) 667.
[22] J.M. Criado, J. Morales, Thermochim. Acta 19 (1977) 305.
[23] J.M. Criado, J. Morales, V. Rives, J. Therm. Anal. 14 (1978) 221.
[24] A.W. Coats, J.P. Redfern, Nature 201 (1964) 68.
[25] P. Budrugeac, Polym. Degrad. Stab. 71 (2001) 185.
[26] M. Nakajima, S. Shimizu, K. Onuki, Y. Ikezoe, S. Sato, Chem. Soc. Jpn. 4 (1989) 681.
[27] S.V. Vyazovkin, V. Goryachko, A.I. Lesnikovich, Thermochim. Acta 197 (1992) 41.
[28] N. Koga, J. Šesták, J. Therm. Anal. 37 (1991) 1103.
[29] N. Koga, J. Šesták, J. Málek, Thermochim. Acta 182 (1991) 333.
[30] J.M. Criado, J. Therm. Anal. 21 (1981) 155.
[31] J. Šesták, J. Therm. Anal. 37 (1991) 111.
[32] J. Šesták, G. Berggren, Thermochim. Acta 3 (1971) 1.
[33] J. Málek, Thermochim. Acta 138 (1989) 337.
[34] J. Málek, J.M. Criado, J. Šesták, J. Militký, Thermochim. Acta 153 (1989) 429.
[35] V.M. Gorbachev, J. Therm. Anal. 18 (1980) 13.
[36] J. Málek, Y. Messaddeq, S. Inoue, T. Mitsuhashi, J. Mater. Sci. 30 (1995) 3082.
[37] J. Šesták, J. Málek, Solid State Ionics. 63–65 (1993) 245.
[38] J. Šesták, V. Šatava, W. Wendlandt, Thermochim. Acta 7 (1973) 333.